



## Hydrogenation of pyrene using Pd catalysts supported on tungstated metal oxides

Qiang Lin, Ken-ichi Shimizu, Atsushi Satsuma\*

Graduate School of Engineering, Nagoya University, Chikusa-ku, Nagoya 464-8603, Japan

### ARTICLE INFO

#### Article history:

Received 18 May 2010

Received in revised form 6 August 2010

Accepted 11 August 2010

Available online 17 August 2010

#### Keywords:

Solid acid

Pd catalysts

Hydrogenation

Pyrene

Tungstated metal oxides

UV-visible spectroscopy

### ABSTRACT

A series of Pd catalyst supported on tungstated metal oxides (Pd/W–MO<sub>x</sub>) were prepared and applied for pyrene hydrogenation, and the role of acid sites of supports was investigated. Among Pd/W–MO<sub>x</sub> catalysts, Pd/W–TiO<sub>2</sub> showed the highest activity which was comparable to those of Pd/BEA, Pd/Y and Pd/SiO<sub>2</sub>–Al<sub>2</sub>O<sub>3</sub>. As for the Pd catalysts supported on metal oxides without tungstate (Pd/MO<sub>x</sub>), the hydrogenation activity became higher with the increase in the acid amount of supports measured by calorimetric measurement of ammonia adsorption. The important role of acid sites on hydrogenation activity was demonstrated. On the other hand, the hydrogenation activity of Pd/W–MO<sub>x</sub> catalysts was not correlated to the acid amount of supports measured by ammonia adsorption. On-site generation of protonic acid on tungstated metal oxide supports was estimated from kinetic analysis of reduced W species in the presence of hydrogen by *in situ* UV–visible measurement. From a good correlation between the kinetic parameters of on-site protonic acid formation and the hydrogenation activity, the important role of protonic acid formation on tungstated metal oxide supports was clarified.

© 2010 Elsevier B.V. All rights reserved.

### 1. Introduction

High aromatic content in diesel fuel lowers the fuel quality and contributes significantly to the formation of undesired emissions in exhaust gases [1–7]. As a simple solution to remove the aromatics, deep hydrogenation of aromatic hydrocarbons over supported noble metal catalysts in mild conditions has drawn much attention [1,2]. Metal oxides having strong acidity is known to be effective as supports of noble metals [1,3,6]. Due to their strong acidity, zeolites are the attractive materials for supports [3,6,8–12]. However, the pore sizes are usually too small to allow access of polycyclic aromatic hydrocarbons. Actually, the minimum cross-sectional diameters of the aromatic molecules in diesel fuels are much larger than the pore-mouth opening of the supercage of Y zeolite [13]. One of the solutions to overcome the large barrier of aromatics is the introduction of meso- or macropores to zeolite crystals [13–16]. For example, Tang et al. [15] showed that mesoporous-loaded Pd/BEA (mesoporous volume of 0.17 cm<sup>3</sup> g<sup>-1</sup>) represented higher activity for pyrene hydrogenation than normal Pd/BEA (mesoporous volume of 0.06 cm<sup>3</sup> g<sup>-1</sup>), though the surface area and the acid amount of the supports were comparable. Due to the merit of diffusion of polycyclic aromatics, mesoporous silicas or amorphous silica–alumina are also preferable as a support for noble metals [16–19].

The main reasons for the use of silicates and alumina as supports for hydrogenation catalysts are their high surface area and the greater acidity. Actually, the important role of the acid sites of supports has been well investigated [6,9,11,12,18,19]. Yasuda et al. [11] investigated the effect of SiO<sub>2</sub>/Al<sub>2</sub>O<sub>3</sub> ratio of USY zeolites as supports for Pd–Pt bimetallic catalysts, and reported that the activity for tetralin hydrogenation was strongly dependent on the SiO<sub>2</sub>/Al<sub>2</sub>O<sub>3</sub> ratio. Zheng et al. [12] also examined the effect of SiO<sub>2</sub>/Al<sub>2</sub>O<sub>3</sub> ratio of Pd/USY on the hydrogenation of naphthalene. They found the decrease of the hydrogenation activity with the increase of SiO<sub>2</sub>/Al<sub>2</sub>O<sub>3</sub> ratio was in harmony with the acid amount of USY determined by *n*-buthylamine-temperature programmed desorption. Pawelec et al. compared the hydrogenation activity of Pd/BEA, Pd/SiO<sub>2</sub>–Al<sub>2</sub>O<sub>3</sub>, and Pd/Al<sub>2</sub>O<sub>3</sub> using a model feed containing toluene, naphthalene and dibenzothiophene [18], respectively. They concluded that the highest hydrogenation activity of Pd/SiO<sub>2</sub>–Al<sub>2</sub>O<sub>3</sub> can be attributed to the greater Brønsted acidity of Pd/SiO<sub>2</sub>–Al<sub>2</sub>O<sub>3</sub> and the degree of reduction of Pd species. The positive role of acid sites of supports were attributed to both the hydrogen spill-over mechanism and the electron-deficient state of supported noble metals on acidic supports [6,12,18]. However, such investigations on the role of acidity have been limited in the silicates and alumina.

As described above, the promotional role of silicate supports on the hydrogenation is essentially based on their greater amount of strong acid sites. Other materials, such as transition metal oxides, having strong acid sites would be other candidates for the supports of precious metals for the hydrogenation of polycyclic aromatics.

\* Corresponding author. Tel.: +81 52 789 4608; fax: +81 52 789 3193.

E-mail address: [satsuma@apchem.nagoya-u.ac.jp](mailto:satsuma@apchem.nagoya-u.ac.jp) (A. Satsuma).

**Table 1**

List of tungstated metal oxides prepared in the present study.

Abbreviation	Tungstated metal oxides	W concentration (wt.% of WO <sub>3</sub> )	Surface area (m <sup>2</sup> g <sup>-1</sup> )	Surface W density (nm <sup>-2</sup> )
10WZ	WO <sub>3</sub> /ZrO <sub>2</sub>	10	105	2.5
25WZ	WO <sub>3</sub> /ZrO <sub>2</sub>	25	108	6.0
45WZ	WO <sub>3</sub> /ZrO <sub>2</sub>	45	101	11.6
WMg	WO <sub>3</sub> /MgO	18	98	4.8
WTi	WO <sub>3</sub> /TiO <sub>2</sub>	9	46	5.0
WAl	WO <sub>3</sub> /Al <sub>2</sub> O <sub>3</sub>	30	178	4.3
WCe	WO <sub>3</sub> /CeO <sub>2</sub>	10	53	4.8

In the present study, we apply tungstated metal oxides as supports of Pd catalysts for the hydrogenation of pyrene. Tungstated metal oxides, such as WO<sub>3</sub>/ZrO<sub>2</sub>, are well known as solid acid materials which can be applied for various applications such as hydrodesulfurization, hydrocarbon cracking and light alkane isomerization [20–23]. It has been reported that the types of oxide support and the supported W density on the surface affect the amount and strength of acid sites on tungstated metal oxides [20–26]. Due to their redox property, supported tungstate is reduced in the presence of hydrogen to form partially reduced W species involving simultaneous formation of protonic acids, i.e., Brønsted acids [21–29]. This process can be significantly enhanced by an introduction of noble metals [25,30]. Therefore, promotion effect of tungstated metal oxides can be expected in the hydrogenation reactions.

The aims of this study are to clarify (1) the potential of tungstated metal oxides as supports of Pd catalysts for the hydrogenation of polycyclic aromatic hydrocarbons and (2) the role of solid acid on tungstated metal oxides for the hydrogenation reaction. Pyrene is used as a typical model compound of polycyclic aromatic hydrocarbons. The following two techniques are applied to estimate the acid sites of supports; (1) a microcalorimetric measurement of NH<sub>3</sub> adsorption and (2) a kinetic analysis of surface tungstate using *in situ* UV–visible spectroscopy for estimation of on-site formation of protonic acids in the presence of hydrogen [30].

## 2. Experimental

### 2.1. Preparation of tungstated metal oxides

ZrO<sub>2</sub> was prepared by hydrolysis of zirconium oxynitrate 2-hydrate in distilled water by gradually adding an aqueous NH<sub>4</sub>OH solution (1.0 mol dm<sup>-3</sup>), filtration of precipitate, washing with distilled water three times, and dryness at 373 K.  $\gamma$ -Al<sub>2</sub>O<sub>3</sub> was prepared by calcination of  $\gamma$ -AlOOH (Catapal B Alumina purchased from Sasol) at 873 K for 3 h. Tungsten oxide (WO<sub>3</sub>, 99.9%, 16 m<sup>2</sup> g<sup>-1</sup>) is supplied by Kishida Chemical Co. Ltd. Amorphous silica (JRC-SIO-8, 303 m<sup>2</sup> g<sup>-1</sup>), TiO<sub>2</sub> (JRC-TiO-4, 50 m<sup>2</sup> g<sup>-1</sup>), MgO (JRC-MGO-1, 180 m<sup>2</sup> g<sup>-1</sup>) and CeO<sub>2</sub> (JRC-CeO-1, 53 m<sup>2</sup> g<sup>-1</sup>) were supplied from the Catalysis Society of Japan. Tungstated metal oxides were prepared by impregnation of an aqueous solution of ammonium paratungstate with above-mentioned supports. Samples were dried at 373 K overnight and then calcined in ambient air at 873 K for 3 h. The properties and abbreviations of tungstated metal oxides are listed in Table 1.

### 2.2. Preparation of Pd-supported catalysts

In addition to above-mentioned metal oxides and tungstated metal oxides, proton-type Y zeolite (Y, JRC-Z-HY4.8, SiO<sub>2</sub>/Al<sub>2</sub>O<sub>3</sub> = 4.8), proton-type BEA zeolite (BEA, JRC-Z-HB25, SiO<sub>2</sub>/Al<sub>2</sub>O<sub>3</sub> = 25) and SiO<sub>2</sub>-Al<sub>2</sub>O<sub>3</sub> (JRC-SAL-2, SiO<sub>2</sub>/Al<sub>2</sub>O<sub>3</sub> = 5.6, 560 m<sup>2</sup> g<sup>-1</sup>) supplied from the Catalysis Society of Japan were used as supports. Supported Pd catalysts with Pd loading of 0.02 wt.% were prepared by impregnation of an aqueous solution

of Pd(NH<sub>3</sub>)<sub>4</sub>Cl<sub>2</sub> with these supports, followed by drying at 373 K overnight, and calcination in air at 723 K for 2 h.

### 2.3. Characterization

BET surface areas were measured using a flow apparatus for N<sub>2</sub> adsorption at 77 K according to the one-point method. Microcalorimetric measurement on NH<sub>3</sub> adsorption was performed at 423 K using a microcalorimeter (Tokyo Rikou Co., HAC-450G). Before the adsorption experiments, the sample (0.1 g) was pretreated under vacuum for 6 h at 423 K.

Diffuse reflectance UV–visible measurements were made using a UV–visible spectrometer (JASCO V-550) equipped with an *in situ* flow cell having a quartz window, a heating system inside, and connected with a gas flow system as reported in our previous paper [30]. A thermocouple located under the bed of the sample cell was used to measure the local temperature. The light source is led to the center of an integrating sphere by an optical fiber. Reflectance was converted to pseudo-absorbance using the Kubelka-Munk function. BaSO<sub>4</sub> was used to collect a background spectrum. Model gas mixtures were fed at a flow rate of 100 cm<sup>3</sup> min<sup>-1</sup> to supported tungsten oxide samples (50 mg) which were pretreated in a flow of O<sub>2</sub> (10%)/He at 823 K for 20 min. Then the time resolved *in situ* UV–visible spectra were recorded at 473 K.

## 3. Hydrogenation of pyrene

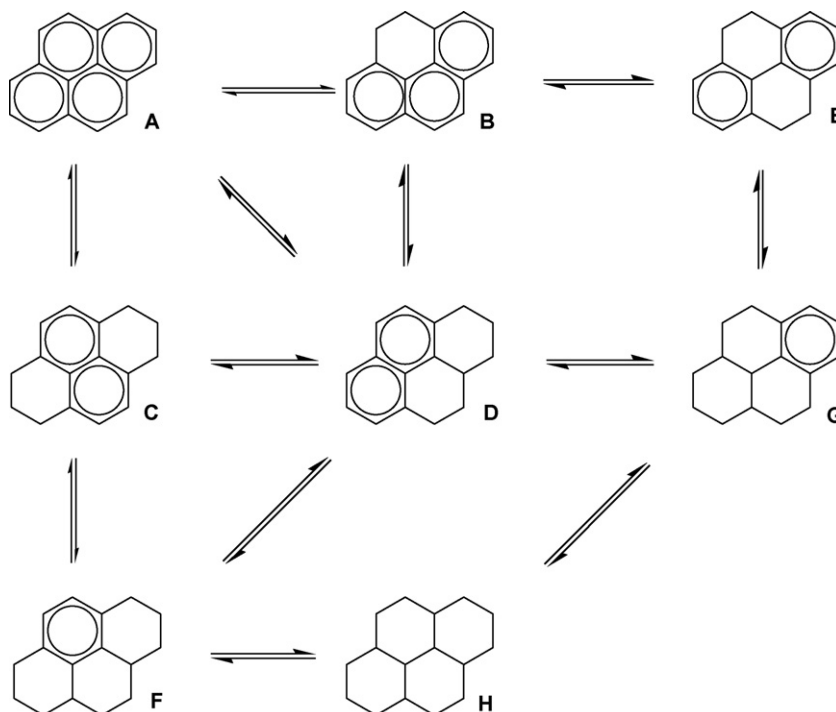
The hydrogenation of pyrene was carried out in a batch stainless autoclave having a diameter of 2 cm and a volume of 40 mL. In a typical run of reaction, the reaction conditions were as follows: a 0.1 g of catalyst, 1 mmol of pyrene in 4 mL of *n*-decane, reaction temperature of 523 K, initial total pressure of 6.2 MPa (hydrogen pressure of about 6.0 MPa), reaction time of 80 min, and stirring rate of 800 rpm. Liquid products were analyzed by GC-FID (Shimadzu GC-14A) and GC-MS (Shimadzu GC-17A) with Rtx-65 or DB-1 capillary column (Shimadzu). The yields of products were determined by quantitative GC analysis using *n*-dodecane as an internal standard, and the conversion was determined by the sum of the yields. Average material balance, estimated from comparison of the total yield and the amount of recovered pyrene, was 90.4%.

The reaction network of pyrene hydrogenation has been proposed as Fig. 1 [15,31]. Pyrene hydrogenation is a consecutive reaction that creates products in the order of dihydroxyrene (B), tetrahydroxyrene (E), hexahydroxyrene (C and D), decahydroxyrene (G and F) and perhydroxyrene (H). It was also reported that the rate of the first ring hydrogenation is fast, the hydrogenation rate gradually decreases with the hydrogenation getting deeper, and the hydrogenation of the last ring is very difficult [1,15,16,31].

## 4. Result and discussion

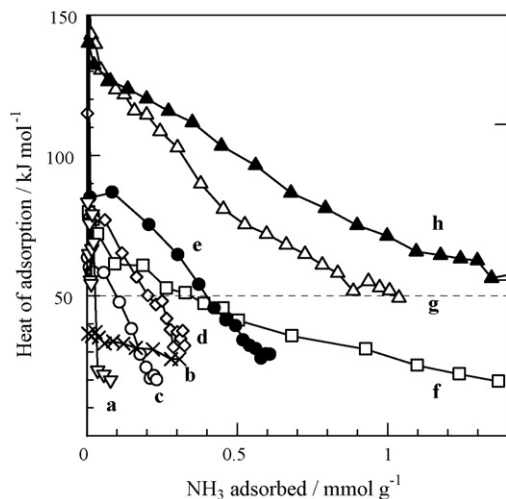
### 4.1. Acidic properties of support

Fig. 2 shows the profiles of the differential heat of NH<sub>3</sub> adsorption on various supports. BEA and Y zeolites show the initial



**Fig. 1.** Proposed network of pyrene hydrogenation: (A) pyrene, (B) 4,5-dihydropyrene, (C) 1,2,3,6,7,8-hexahydropyrene, (D) 1,2,3,3a,4,5-hexahydropyrene, (E) 4,5,9,10-tetrahydropyrene, (F) 1,2,3,3a,4,5,5a,6,7,8-decahydropyrene, (G) 1,2,3,3a,4,5,9,10,10a,10b-decahydropyrene and (H) perhydropyrene.

heat of adsorption in the range of 130–150 kJ mol<sup>-1</sup>, which are in agreement with previous reports [32–34]. The differential heat of adsorption gradually decreases with the loading amounts of NH<sub>3</sub>, and finally reaches to around 50 kJ mol<sup>-1</sup> above the surface coverage of 1.0 mmol g<sup>-1</sup>. Since this minimum heat of adsorption can be assigned to hydrogen-bonded NH<sub>3</sub>, we have defined the total acid amount from adsorbed NH<sub>3</sub> having the differential heat above 50 kJ mol<sup>-1</sup>. Tungstated metal oxides show the initial heat of adsorption in the range of 60–90 kJ mol<sup>-1</sup>. Other metal oxides (not shown), i.e. Al<sub>2</sub>O<sub>3</sub>, TiO<sub>2</sub> and ZrO<sub>2</sub>, showed the initial heat of adsorption in the range of 60–90 kJ mol<sup>-1</sup>. On the other hand, the initial heat of adsorption on SiO<sub>2</sub> is only 37 kJ mol<sup>-1</sup>, which is due to weak adsorption of NH<sub>3</sub> via hydrogen-bonding [35]. The amounts of acid site on all the supports thus determined are summarized in Table 2.



**Fig. 2.** Differential heat of adsorption of NH<sub>3</sub> on (a) WMg, (b) SiO<sub>2</sub>, (c) WTi, (d) 25WZr, (e) WAl, (f) SiO<sub>2</sub>-Al<sub>2</sub>O<sub>3</sub>, (g) BEA zeolite and (h) Y zeolite.

#### 4.2. Catalytic hydrogenation

Table 2 shows the results of catalytic tests for pyrene hydrogenation over various supported Pd catalysts. When WZ samples are used as supports, the catalytic activity is strongly affected by WO<sub>3</sub> content (Runs 1–3). Pd/25WZ shows the highest pyrene conversion of 56.6% among these three catalysts. Taking the surface area of ZrO<sub>2</sub> into account, WO<sub>3</sub> content of 25 wt.% is nearly the theoretical monolayer W density (7 W nm<sup>-2</sup>). As we have reported, supported WO<sub>3</sub> is present as surface polytungstates and tungsten oxo-clusters up to the theoretical monolayer W density, and the further increase in the WO<sub>3</sub> content results in the formation of crystalline WO<sub>3</sub> [30]. The decrease in the pyrene conversion at Pd/45WZ suggests that the presence of WO<sub>3</sub> crystalline is not favorable.

The effect of supports on tungstated metal oxides having the theoretical monolayer W density is compared in the Runs 2 and 4–7. This series of catalysts is abbreviated as Pd/W-MOX, hereafter. Among the series of catalysts, Pd/WTi shows the highest conversion (76.9%). It should be noted that the conversion of pyrene hydrogenation over Pd/WTi is comparable to those of the state-of-the-art catalysts, i.e., Pd/SiO<sub>2</sub>-Al<sub>2</sub>O<sub>3</sub>, Pd/Y and Pd/BEA (Runs 8–10).

The pyrene conversion on Pd/25WZ, Pd/WAl and Pd/WTi are higher than those on Pd/ZrO<sub>2</sub>, Pd/Al<sub>2</sub>O<sub>3</sub> and Pd/TiO<sub>2</sub>, respectively. The addition of WO<sub>3</sub> generally enhances the hydrogenation activity. This is contrary to the results reported by Albertazzi et al. [36–38]. They reported that addition of WO<sub>3</sub> onto TiO<sub>2</sub> decreased the catalytic activity for tetralin hydrogenation on 1 wt.% Pd/Pt supported catalysts. In this study, Pd loading is 0.02 wt.% and far lower than that of their study. The difference in the effect of WO<sub>3</sub> addition may be due to the content of noble metals. The lower content of Pd in this study is preferable for the positive effects of tungstated metal oxides.

The amount of H<sub>2</sub> consumption for various catalysts in Table 2 was calculated from the sum of produced dihydropyrenes. Obviously, higher pyrene conversion leads to broader distribution of products and higher selectivity of deeply hydrogenated products (C, D, F and G). It should be noted that zeolite-supported Pd catalysts,

**Table 2**Conversion and selectivity for hydrogenation of pyrene over various supported Pd catalysts<sup>a</sup>.

Run	Catalysts	Pyrene Conv. (%)	Product selectivity (%)								H <sub>2</sub> consumption <sup>c</sup> (mmol)	Acid amount <sup>d</sup> (mmol g <sup>-1</sup> )
			B	C	D	E	F	G	H	Others <sup>b</sup>		
1	Pd/10WZr	48.0	35.1	2.1	1.2	9.4	0.2	–	–	–	0.73	0.13
2	Pd/25WZr	56.6	40.8	2.7	1.5	11.3	0.2	0.1	–	–	0.78	0.20
3	Pd/45WZr	35.7	27.3	1.0	0.6	6.7	0.1	–	–	–	0.51	0.14
4	Pd/WMg	15.8	13.7	0.3	0.2	1.6	–	–	–	–	0.20	0.02
5	Pd/WCe	35.1	26.9	1.3	0.7	6.2	–	–	–	–	0.51	0.07
6	Pd/WAl	52.6	40.2	1.4	0.7	9.3	1.0	–	–	–	0.66	0.40
7	Pd/WTi	76.9	42.1	8.4	3.0	22.2	0.7	0.5	–	–	1.27	0.10
8	Pd/SiO <sub>2</sub> –Al <sub>2</sub> O <sub>3</sub>	78.6	38.7	8.9	4.8	23.1	2.1	1.0	–	–	1.58	0.33
9	Pd/Y	68.4	37.3	7.3	3.2	16.4	0.8	0.4	–	3.0	1.09	1.45
10	Pd/BEA	84.2	36.8	3.5	3.5	19.3	1.7	1.0	–	18.4	1.11	1.00
11	Pd/Al <sub>2</sub> O <sub>3</sub>	19.8	14.6	0.8	0.5	3.9	–	–	–	–	0.27	0.05
12	Pd/TiO <sub>2</sub>	13.4	12.0	0.3	–	1.1	–	–	–	–	0.15	0.02
13	Pd/WO <sub>3</sub>	12.4	8.8	0.5	0.3	2.8	–	–	–	–	0.19	0.02
14	Pd/SiO <sub>2</sub>	9.4	6.4	0.2	–	2.8	–	–	–	–	0.14	0.00
15	Pd/ZrO <sub>2</sub>	5.3	4.4	–	–	0.9	–	–	–	–	0.07	0.01

<sup>a</sup> Reaction conditions: temperature, 523 K; initial total pressure, 6.2 MPa; reaction time, 80 min.<sup>b</sup> Major products are ring opening derivatives from pyrene.<sup>c</sup> Calculated from sum of H<sub>2</sub> consumed on pyrene hydrogenation products from B to H in Fig. 1.<sup>d</sup> Acid amount of support determined from heat of NH<sub>3</sub> adsorption.

Pd/Y and Pd/BEA, produced some other products of higher molecular mass, which were assigned mainly to hydro-benzopyrenes or alkyl-pyrenes by using GC–MS. Because they are produced through alkylation of pyrene and the solvent of decane on acid sites of zeolites, the influence of these by-products on hydrogenation on Pd surface should be negligible. Therefore, the amount of H<sub>2</sub> consumption estimated from hydro-pyrene yield can be regarded as a measure of both the hydrogenation activity and selectivity.

In the case of Pd catalysts supported on the simple metal oxides (Runs 11–15), the H<sub>2</sub> consumptions are correlated with the amount of acid sites, i.e., the highest H<sub>2</sub> consumption is observed on Pd/Al<sub>2</sub>O<sub>3</sub>, while Pd/SiO<sub>2</sub> and Pd/ZrO<sub>2</sub> show very low activity. The H<sub>2</sub> consumption is more than 6 times higher on more acidic Pd/SiO<sub>2</sub>–Al<sub>2</sub>O<sub>3</sub> catalyst than that of Pd/Al<sub>2</sub>O<sub>3</sub>. However, this correlation cannot be observed in other series of catalysts. For example, Pd/WTi is the most active among Pd/W–MOx catalysts but its acid amount estimated by calorimeter is very low (0.10 mmol g<sup>-1</sup>). The zeolite-supported Pd catalysts also show lower hydrogenation activities than that of Pd/SiO<sub>2</sub>–Al<sub>2</sub>O<sub>3</sub>, although they have larger amount of acid sites. The dependence of pyrene hydrogenation on the acidity of support will be discussed in the next section.

#### 4.3. Effect of acid sites on hydrogenation

The H<sub>2</sub> consumption over the supported Pd catalysts are plotted in Fig. 3 as a function of the amount of acid sites on the supports estimated by the differential heat of NH<sub>3</sub> adsorption. In the cases of Pd-supported on SiO<sub>2</sub>–Al<sub>2</sub>O<sub>3</sub>, Al<sub>2</sub>O<sub>3</sub>, TiO<sub>2</sub>, WO<sub>3</sub>, SiO<sub>2</sub> and ZrO<sub>2</sub> (abbreviated as Pd/MOx, hereafter), the H<sub>2</sub> consumption is fairly correlated with the amount of acid sites as shown in the straight line in the figure. This result suggests the hydrogenation activity is strongly influenced by the acidity of supports for metal-supported catalysts with a low content of Pd (0.02 wt.%). Although it is well known that benzene hydrogenation proceeds via a purely metal catalyzed reaction [1], the important role of acid sites on supports also been pointed out for hydrogenation of aromatics over silicates and alumina [6,11,16,24,27]. Quantitative correlation between the acid amount and the hydrogenation activity was reported by Pawelec et al. [6,18]. As proposed by Vannice and co-workers [39–41] and other researchers [27,42,43], acid sites can produce protons from spill-over hydrogen migrated from metal surface, which can activate aromatic molecules adsorbed on acidic sites by the formation of carbocation. Wang et al. suggested that the hydrogenation

reaction could take place on metal sites as well as on acid sites over noble metal/acid zeolite catalysts [27]. Furthermore, Simon et al. proposed that benzene hydrogenation over 1.0 or 1.1 wt.% Pt/mordenites includes two routes: (i) the monofunctional hydrogenation of benzene on the metal itself and (ii) the hydrogenation of Brønsted acid bound benzene using hydrogen dissociated on the metal surface nearby [42]. They also showed a model that the hydrogenation mainly proceeds via acidic path when the activity of the metal sites decreased during surface Pt metal poisoned by thiophene. Accordingly, in the case of our catalysts with only small Pd loading, the acidic pathway mainly contributes to hydrogenation of aromatic molecules. As shown in the correlation of Pd/MOx in Fig. 3, the promotion effect of solid acids on the hydrogenation activity is confirmed in the case of Pd catalysts supported on the transition metal oxides. This result suggests that the possible reaction pathway should be similar to the proposals of Vannice and co-workers [39–41] and Simon et al. [42]. The hydrogenation mainly proceeds as adsorption and then activation of pyrene on Brønsted acid sites to form carbocation intermediate followed by hydrogenation using dissociated hydrogen atoms migrated from metal surface

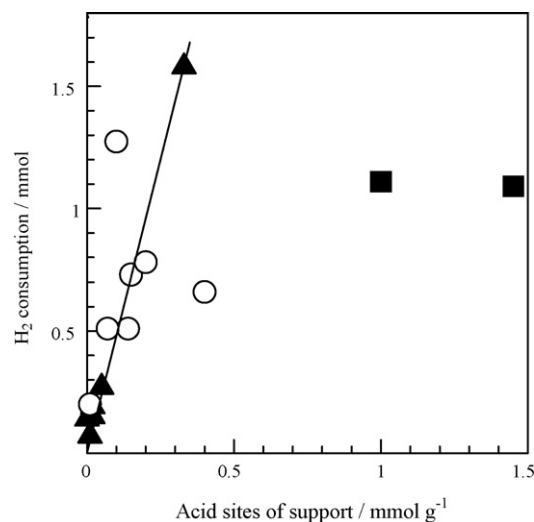


**Fig. 3.** H<sub>2</sub> consumptions for pyrene hydrogenation over Pd catalysts supported on (■) zeolites, (○) tungstated metal oxides and (▲) other metal oxides.

or hydride. The formation of hydride on acidic supports is proposed by Hattori and Shishido [44] as follows. The hydrogen molecule dissociates on metal surface and hydrogen atoms spill-over onto the acidic support and migrate to Lewis acid sites, where the hydrogen atom releases an electron to become a proton. The electron trapped on the Lewis acid site may react with a second hydrogen atom to form a hydride which is stabilized on the Lewis acid site.

Although the amounts of acid site are very high on Pd/Y and Pd/BEA, these catalysts show lower H<sub>2</sub> consumptions than that of Pd/WTi and Pd/SiO<sub>2</sub>-Al<sub>2</sub>O<sub>3</sub>. This result suggests a negative effect of diffusion limitation of pyrene and hydroxyrenes in the zeolite channel. This is because the molecular diameter of pyrene (0.72–0.92 nm in its planer directions) is larger than the pore diameter of Y (0.74 nm) and BEA (0.66–0.77 nm). Actually, Meng et al. [13] and Zhang et al. [16] reported that the introduction of mesopores into zeolite Y results in the higher hydrogenation activity for naphthalene and pyrene over Pd–Pt/Y, respectively. Tang et al. [15] also demonstrated that the pyrene hydrogenation activity was promoted by the increase in the mesoporous volume of Pd/BEA. These results indicate the diffusion limitation of aromatic compounds to access the acid sites or metal clusters in zeolite micropores. In the present study, the lower hydrogenation activity of Pd/Y and Pd/BEA than that expected from the acid amount of supports can be rationalized by the diffusion limitation of pyrene and hydroxyrenes in the zeolite channels.

As shown in open circles in Fig. 3, the correlation between the H<sub>2</sub> consumption and the amount of acid site is not clear on Pd/W–MOx, indicating that other controlling factors work for the pyrene hydrogenation activity. The influence of diffusion limitation can be excluded because the surface areas of Pd/W–MOx are comparable or lower than those of Pd/MOx. It can be expected that some chemical properties of surface W species affected the activity for pyrene hydrogenation. As a characteristic function of WO<sub>3</sub>/ZrO<sub>2</sub>, it is well known that protonic acid sites, i.e., Brønsted acid sites, are formed from gaseous hydrogen molecules involving reduction of surface W<sup>6+</sup> to W<sup>(6-δ)+</sup> [21–29]. This reduction–oxidation process including the formation of protonic acids can be simply expressed as the following Eq. (1) [30]:



These temporary protonic acids act as active Brønsted acids to catalyze *o*-xylene or *n*-alkane isomerization in the presence of H<sub>2</sub> [24]. Furthermore, the addition of precious metals on solid acids generally promotes the formation of protonic acid sites [20,25,44]. Actually, a loading of Pt onto WO<sub>3</sub>/ZrO<sub>2</sub> significantly improves isomerization of pentane at lower temperatures [24]. Therefore, the on-site formation of protonic acid sites by H<sub>2</sub> dissociation should affect the catalytic activity of pyrene hydrogenation. In the next section, we will examine the contribution of the on-site formation of protonic acid sites in the pyrene hydrogenation.

#### 4.4. Contribution of on-site formation of protonic acid on pyrene hydrogenation

According to the Eq. (1), the on-site formation of protonic acids over W–MOx can be estimated from the formation of reduced W<sup>(6-δ)+</sup> species. Diffuse reflectance UV–visible spectroscopy is a powerful tool for characterizing the electronic states of surface tungstate species [21–24]. Iglesia and co-workers examined the color centers in WOx domains during reduction by hydrogen [22,24]. In the previous paper, we reported an kinetic analysis of the reduction–oxidation process between surface W<sup>6+</sup> and W<sup>(6-δ)+</sup> species using time resolved *in situ* UV–visible spectroscopy [30]. In this study, we apply the time resolved *in situ* UV–visible spec-

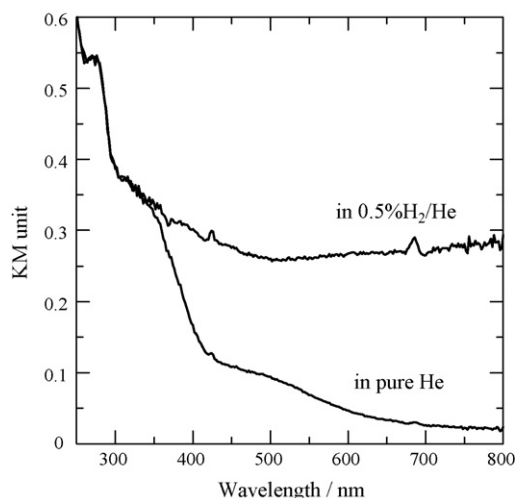
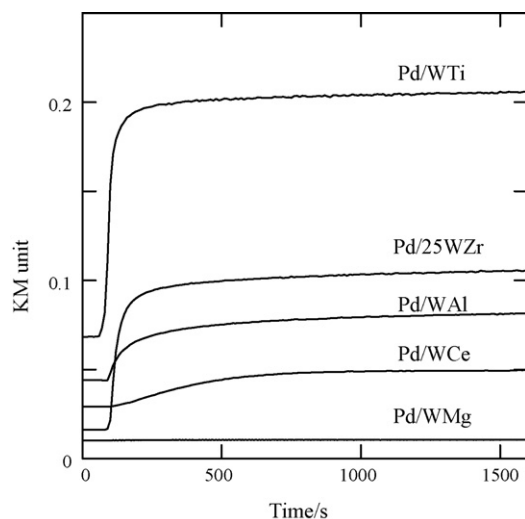


Fig. 4. UV–vis spectra of Pd/25WZr in a flow of pure He and 0.5% H<sub>2</sub>/He at 473 K.

troscopy for the estimation of the on-site formation of protonic acids on Pd/W–MOx catalysts.

Fig. 4 shows UV–visible spectra of Pd/25WZr in a flow of 0.5% H<sub>2</sub>/He and pure He at 473 K after pretreatment in a flow of O<sub>2</sub>/He at 823 K and cooling to 473 K in flowing He. In pure He, Pd/25WZr shows only a major broad band below 410 nm assigned to the LMCT band of tungstate [23,30]. When the catalyst reduced in a flow of 0.5% H<sub>2</sub>/He, another broad band appears in the range of 350–800 nm together with the LMCT band below 410 nm. After the switching the flow gas from H<sub>2</sub>/He to pure He, the broad band gradually decreases and finally returns to the original level (figure not shown). Since the UV–visible spectra of pure ZrO<sub>2</sub> gave no absorption band in the range of 350–800 nm under both oxidative and reductive atmospheres, oxidation state of ZrO<sub>2</sub> do not affect the spectra of Pd/25WZr. For pure CeO<sub>2</sub>, the change in the band intensity in the same range was less than 0.001 KM unit between the oxidative and reductive atmospheres. The negligible contribution of supported 0.02 wt.% of Pd to the spectra of Pd/W–MOx was also confirmed by a set of separate experiments. For example, the sample of 0.02 wt.% Pd/ZrO<sub>2</sub> without WO<sub>3</sub> only showed very small absorption band below 0.02 KM unit in the range of 300–800 nm and below 0.0035 KM unit at 600 nm, and the change in the band intensity was only below 0.004 KM unit with the reduction in 0.5% H<sub>2</sub>/He. Therefore, the change in the band intensity in the range of 350–800 nm represents the reduction–oxidation process between surface W<sup>6+</sup> and W<sup>(6-δ)+</sup> species. Although the pyrene hydrogenation was carried out at 523 K, the *in situ* UV–visible measurements were carried out at 473 K because a part of surface tungstate was irreversibly reduced at 523 K but all the surface tungstate reversibly reduced and oxidized at 473 K.

Fig. 5 shows the transient response of the band at 600 nm of Pd/W–MOx catalysts in a flow of pure He (0–50 s) and 0.5% H<sub>2</sub>/He (after 50 s) at 473 K. As shown in the figure, the band intensity at 600 nm initially increases after the feed of 0.5% H<sub>2</sub>/He due to the reduction of surface W<sup>6+</sup> to W<sup>(6-δ)+</sup> species, and then reaches to the equilibrium [30]. It is clear that the response magnitude of the band is the greatest on Pd/WTi, and Pd/25WZr also show a large change in the band intensity. On the other hand, the reduction of surface W species is negligible on Pd/WMg. The maximum response magnitude between the oxidized state and the equilibrium in 0.5% H<sub>2</sub>/He, indicated as ΔKM hereafter, is in the order of Pd/WTi > Pd/WZr > Pd/WAl > Pd/WCe > Pd/WMg. When the flowing gas was switched to pure He, the intensity of the band decreased by re-oxidation of W<sup>(6-δ)+</sup> to W<sup>6+</sup> species, as reported in the previous paper (figure not shown) [30].



**Fig. 5.** Transient response of the band at 600 nm of Pd/W–MOx catalysts at 473 K. The flowing gas was switched from pure He to 0.5%H<sub>2</sub>/He at 50 s.

As reported in the previous paper [30], the rate constants of reduction ( $k_R$ ) and that of re-oxidation ( $k_O$ ) in Eq. (1) were estimated from the responses of the band in the initial stage of the reduction or the re-oxidation using the following first-order reaction equation:

$$kt = \ln[W^{(6-\delta)+}] - \ln[W^{(6-\delta)+}_0] \quad (2)$$

Table 3 summarizes the rate constants of reduction ( $k_R$ ) and re-oxidation ( $k_O$ ), their ratio ( $k_R/k_O$ ), and  $\Delta KM$ . These parameters are strongly affected by the type of oxide supports. The rate constants of  $k_R$  and  $k_O$  increased in the order of Pd/WMg < Pd/WCe < Pd/WAl < Pd/WZr < Pd/WTi. Since the variation of the rate constant of  $k_R$  is more significant, the ratio of  $k_R/k_O$ , which is the equilibrium constant of the Eq. (1), also increases in the same order. The order of the maximum response magnitude ( $\Delta KM$ ) is also in the same order.

In Fig. 6, the H<sub>2</sub> consumptions for pyrene hydrogenation of Pd/W–MOx catalysts are plotted as a function of  $k_R/k_O$ . As the increase in the equilibrium constant of  $k_R/k_O$ , the H<sub>2</sub> consumption of Pd/W–MOx catalysts increases. Such a good correlation is also observed between the H<sub>2</sub> consumptions and  $\Delta KM$  as shown in Fig. 7, indicating  $\Delta KM$  can be used as more convenient parameter of the equilibrium, alternatively. These correlations clearly demonstrate that the on-site formation of Brønsted acid sites on Pd/W–MOx is the controlling factor for the catalytic activity in the pyrene hydrogenation. This result is in agreement with the discussion for Pd/MOx catalysts in Section 4.3 and also supports the proposed possible mechanism. The on-site formation of Brønsted acid should proceed via dissociative adsorption of a hydrogen molecule on noble metal followed by spill-over of a hydrogen atom and migration on the support surface to form a proton, as proposed by Hattori and co-workers [25,44]. In their proposal, a hydride

**Table 3**

Rate constant of reduction under 0.2%H<sub>2</sub>/He ( $k_R$ ) and re-oxidation under pure He ( $k_O$ ), their ratio ( $k_R/k_O$ ), and change in the band intensity at 600 nm under 0.2%H<sub>2</sub>/He ( $\Delta KM$ ).

Catalyst	$k_R$ (s <sup>-1</sup> )	$k_O$ (s <sup>-1</sup> )	$k_R/k_O$	$\Delta KM$
Pd/WMg	$1.1 \times 10^{-6}$	$1.9 \times 10^{-5}$	0.06	0.0004
Pd/WCe	$4.6 \times 10^{-5}$	$2.8 \times 10^{-4}$	0.16	0.02
Pd/WAl	$2.9 \times 10^{-4}$	$5.8 \times 10^{-4}$	0.50	0.035
Pd/25WZr	$1.5 \times 10^{-3}$	$1.2 \times 10^{-3}$	1.2	0.09
Pd/WTi	$2.7 \times 10^{-3}$	$1.7 \times 10^{-3}$	1.6	0.15

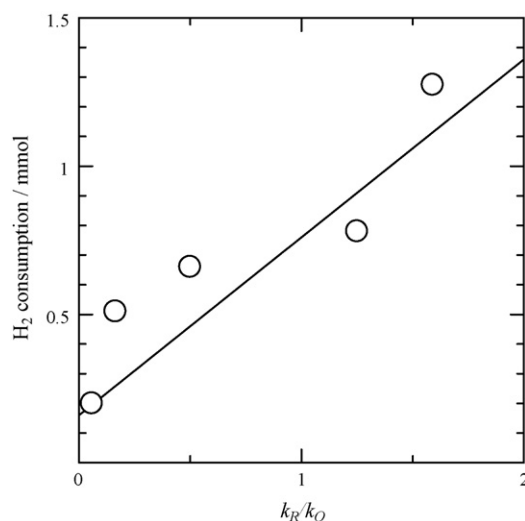


**Fig. 6.** H<sub>2</sub> consumption for pyrene hydrogenation as a function of  $k_R/k_O$  on Pd/W–MOx.

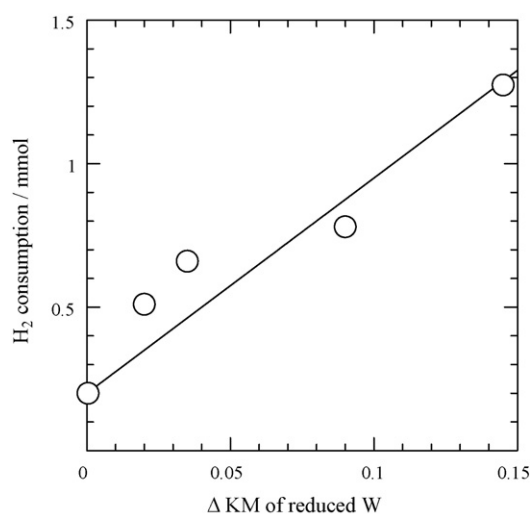


**Fig. 7.** H<sub>2</sub> consumption for pyrene hydrogenation as a function of degree of W reduction on Pd/W–MOx.

should produce via reaction of a hydrogen atom with a trapped electron which was generated with the formation of Brønsted acid on solid supports. In the case of Pd/W–MOx, generation of a hydride could be available via reaction of a spilt hydrogen atom with  $W^{(6-\delta)+}$  species because  $W^{(6-\delta)+}$  species on metal-supported catalysts is easily re-oxidized to  $W^{6+}$  in the presence of noble metal [30]. Consequently, as a characteristic feature of tungstated metal oxide supports, the promoted hydrogenation activities of Pd/W–MOx can be attributed to the on-site formation of protonic acids involving the reduction of  $W^{(6-\delta)+}$  species.

## 5. Conclusion

The effect of acid sites of supports on the pyrene hydrogenation over Pd catalysts was investigated using BEA and Y zeolites, SiO<sub>2</sub>–Al<sub>2</sub>O<sub>3</sub>, Al<sub>2</sub>O<sub>3</sub> and other transition metal oxides, and tungstated metal oxides as supports. Pd/WO<sub>3</sub>–TiO<sub>2</sub> catalyst showed the comparable hydrogenation activity to Pd/BEA, Pd/Y and Pd/SiO<sub>2</sub>–Al<sub>2</sub>O<sub>3</sub>. The catalytic activities of Pd catalysts supported on non-tungstated metal oxides were fairly dependent on the acid amount of supports measured by the heat of NH<sub>3</sub> adsorption. On

the other hand, this correlation was not observed when tungstated metal oxides were used for supports. The hydrogenation activity of Pd/W–MO<sub>x</sub> was well correlated to the equilibrium constant of the reversible reduction–oxidation of the surface W species, which represents the on-site formation of protonic acid from gaseous H<sub>2</sub>. It was concluded that the promoted hydrogenation activities of Pd/W–MO<sub>x</sub> can be attributed to the on-site formation of protonic acids involving the reduction of surface tungstate.

## References

- [1] A. Stanislaus, B.H. Cooper, *Catal. Rev. Sci. Eng.* 36 (1994) 75–123.
- [2] B.H. Cooper, B.B.L. Donnis, *Appl. Catal. A* 137 (1996) 203–223.
- [3] C. Song, X.L. Ma, *Appl. Catal. B* 41 (2003) 207–238.
- [4] D. Minicucci, X.Y. Zou, J.M. Shaw, *Fluid Phase Equilib.* 353 (2002) 194–197.
- [5] T. Yuan, W.D. Marshall, *J. Hazard. Mater. B* 126 (2005) 149–157.
- [6] B. Pawelec, R. Mariscal, R.M. Navarro, S. van Bokhorst, S. Rojas, J.L.G. Fierro, *Appl. Catal. A* 225 (2002) 223–237.
- [7] K.M. Lin, C. Song, *Catal. Today* 31 (1996) 93–104.
- [8] A.D. Schmitz, G. Bowers, C. Song, *Catal. Today* 31 (1996) 45–56.
- [9] C. Song, A.D. Schmitz, *Energy Fuels* 11 (1997) 656–661.
- [10] H. Yasuda, Y. Yoshimura, *Catal. Lett.* 46 (1997) 43–48.
- [11] H. Yasuda, T. Sato, Y. Yoshimura, *Catal. Today* 50 (1999) 63–71.
- [12] J. Zheng, M. Guo, C. Song, *Fuel Process. Technol.* 89 (2008) 467–474.
- [13] X.C. Meng, Y.X. Wu, Y.D. Li, *J. Porous Mater.* 13 (2006) 365–371.
- [14] K.M. Reddy, C. Song, *Catal. Today* 31 (1996) 137–144.
- [15] T. Tang, C. Yin, L. Wang, Y. Ji, F.S. Xiao, *J. Catal.* 249 (2007) 111–115.
- [16] H. Zhang, X. Meng, Y. Li, Y.S. Lin, *Ind. Eng. Chem. Res.* 46 (2007) 4186–4192.
- [17] L.Y. Chen, Z. Ping, G.K. Chuah, S. Jaenicke, G. Simon, *Micropor. Mesopor. Mater.* 27 (1999) 231–242.
- [18] B. Pawelec, J.M. Campos-Martin, E. Cano-Serrano, R.M. Navarro, S. Thomas, J.L.G. Fierro, *Environ. Sci. Technol.* 39 (2005) 3374–3381.
- [19] A. Corma, A. Martínez, V. Martínez-Soriay, *J. Catal.* 169 (1997) 480–489.
- [20] I.E. Wachs, T. Kim, E.I. Ross, *Catal. Today* 116 (2006) 162–168.
- [21] E. Iglesia, D.G. Barton, S.L. Soled, S. Miseo, J.E. Baumgartner, W.E. Gates, G.A. Fuentes, G.D. Meitzner, *Stud. Surf. Sci. Catal.* 101 (1996) 533–542.
- [22] D.G. Barton, S.L. Soled, E. Iglesia, *Top. Catal.* 6 (1998) 87–99.
- [23] D.G. Barton, M. Shtein, R.D. Wilson, S.L. Soled, E. Iglesia, *J. Phys. Chem. B* 103 (1999) 630–640.
- [24] J. Macht, E. Iglesia, *Phys. Chem. Chem. Phys.* 10 (2008) 5331–5343.
- [25] S. Triwahyono, T. Yamada, H. Hattori, *Appl. Catal. A* 242 (2003) 101–109.
- [26] S. Triwahyono, T. Yamada, H. Hattori, *Appl. Catal. A: Gen.* 250 (2003) 65–73.
- [27] J. Wang, Q. Li, J. Yao, *Appl. Catal. A* 184 (1999) 181–188.
- [28] S. Kuba, P. Concepción Heydorn, R.K. Grasselli, B.C. Gates, M. Che, H. Knözinger, *Phys. Chem. Chem. Phys.* 3 (2001) 146–154.
- [29] S. Kuba, P. Lukinskias, R.K. Grasselli, B.C. Gates, H. Knözinger, *J. Catal.* 216 (2003) 353–361.
- [30] Q. Lin, K. Shimizu, A. Satsuma, *Appl. Catal. A* 365 (2009) 55–61.
- [31] S.C. Korre, M.T. Klein, *Ind. Eng. Chem. Res.* 34 (1995) 101–117.
- [32] N. Cardona-Martinez, J.A. Dumesic, *Adv. Catal.* 38 (1992) 149–224.
- [33] A. Auroux, *Top. Catal.* 4 (1997) 71–89.
- [34] V. Solinas, I. Ferino, *Catal. Today* 41 (1998) 179–189.
- [35] K. Shimizu, E. Hayashi, T. Hatamachi, T. Kodama, T. Higuchi, A. Satsuma, Y. Kitayama, *J. Catal.* 231 (2005) 131–138.
- [36] S. Albertazzi, E. Rodríguez-Castellón, M. Livi, A. Jiménez-López, A. Vaccari, *J. Catal.* 228 (2004) 218–224.
- [37] S. Albertazzi, C. Barbieri, A. Infantes-Molina, A. Jiménez-López, R. Moreno-Tost, E. Rodríguez-Castellón, A. Vaccari, *Catal. Lett.* 104 (2005) 29–36.
- [38] S. Albonetti, G. Baldi, A. Barzanti, E.R. Castellon, A.J. Lopez, D.E. Quesada, A. Vaccari, *Catal. Lett.* 108 (2006) 197–207.
- [39] P. Chou, A.A. Vannice, *J. Catal.* 107 (1987) 129–139.
- [40] S.D. Lin, M.A. Vannice, *J. Catal.* 143 (1993), pp. 539–543, 554–562, 563–572.
- [41] D. Poondi, A.A. Vannice, *J. Catal.* 161 (1996) 742–751.
- [42] L.J. Simon, J.G. van Ommen, A. Jentys, J.A. Lercher, *Catal. Today* 73 (2002) 105–112.
- [43] J. Wang, L. Huang, Q. Li, *Appl. Catal. A: Gen.* 175 (1998) 191–199.
- [44] H. Hattori, T. Shishido, *Catal. Surv. Jpn.* 1 (1997) 205–213.